DYNAMICAL EVOLUTION OF NATURAL FORMATIONS IN LIBRATION POINT ORBITS IN A MULTI-BODY REGIME

Aurélie Héritier*

Advanced Concepts Team, ESTEC, PPC-PF, Keplerlaan 1 - 2201 AZ Noordwijk - The Netherlands

Kathleen C. Howell*

School of Aeronautics and Astronautics, Purdue University, West Lafayette, Indiana, 47907, USA

Abstract

This investigation explores the natural dynamics in a multi-body regime for formation flying applications. Natural regions that are suitable to maintain multiple spacecraft in a loose formation are determined in an inertial coordinate frame. Locating a formation of spacecraft in these zones leads to a smaller variation in the mutual distance between the spacecraft and the pointing direction of the formation. These suitable regions approximate quadric surfaces along a reference trajectory and the relationship between the dynamical evolution of the quadric surfaces and the eigenstructure of the reference trajectory is examined.

Keywords: Libration points; Formation flight; Restricted three-body problem

1. Introduction

Spacecraft formations offer many potential applications in the future of space exploration, including the search for habitable terrestrial exoplanets,

*Corresponding author

Email addresses: `Aurelie.Heritier@esa.int` (Aurélie Héritier), `howell@purdue.edu` (Kathleen C. Howell)

the identification of black holes, and many others. During the last decade, due to the detection of a large number of extrasolar planets, new studies on formation flying in multi-body regimes have emerged to support space astronomy. For example, the original New Worlds Observer (NWO) design concept employs a telescope and an external occulter for the detection and characterization of Earth-like planets.(Cash, W. et al., 2011) During the observation of the star, the distance between the two spacecraft and the pointing direction of the formation toward the star line-of-sight are maintained constant. The occulter suppresses the starlight by many orders of magnitude, to enable the observation of habitable terrestrial planets and the detection of life signs.

The L_2 Sun-Earth libration point region has been a popular destination for satellite imaging formations. Barden and Howell investigate the natural behavior on the center manifold near the L_2 Sun-Earth libration point and compute some natural six-spacecraft formations, which demonstrate that quasi-periodic trajectories could be useful for formation flying.(Barten & Howell, 1998) Later, Marchand and Howell extend this study and use some control strategies, continuous and discrete, to maintain non-natural formations near the libration points.(Marchand & Howell, 2005) Space-based observatory and interferometry missions, such as the Terrestrial Planet Finder, have been the motivation for the analysis of many control strategies. Gómez et al. investigate discrete control methods to maintain a formation of spacecraft.(Gómez et al., 2001) Howell and Marchand consider linear optimal control, as applied to nonlinear time-varying systems, as well as nonlinear control techniques, including input and output feedback linearization.(Marchand & Howell, 2005) Hsiao and Scheeres implement position and velocity feedback control laws to force a formation of spacecraft to possess a rotational motion relative to a nominal trajectory. (Hsiao & Scheeres, 2003, 2005) Recently, Gómez et al. derive regions around a halo orbit with zero relative velocity and zero relative radial acceleration that ideally maintain the mutual distances between spacecraft.(Gómez et al., 2005) Most recently, Héritier and Howell then investigate the natural dynamics in the collinear libration point region for the control of formations of spacecraft.(Héritier & Howell, 2011) This current analysis details and expands on the initial work of Héritier and Howell. A more general understanding of these natural regions suitable for formation flight is examined in the inertial frame for the placement of a small formation of spacecraft along various reference trajectories.

Controlling multiple spacecraft in a multi-body environment is challenging and a good understanding of the natural dynamics in this regime is essential.

Hence, this investigation explores the dynamical environment near the L_2 Sun-Earth libration point to aid in the control of a formation of spacecraft, in terms of the relative distance between vehicles. Regions with low natural drift that are suitable to maintain multiple spacecraft in a loose formation are determined in an inertial frame. Locating a formation of spacecraft in these zones leads to a smaller variation in the mutual distance between the spacecraft and the pointing direction of the formation. The characteristics of these zones are then investigated in details. These suitable zones are derived analytically using variational equations relative to the reference path. These regions represent quadric surfaces and the relationship between the dynamical evolution of the quadric surfaces and the eigenstructure of the reference trajectory is examined.

2. Dynamical model

For the analysis of spacecraft formations in a multi-body regime, the Circular Restricted Three-Body Problem (CR3BP) is selected to describe the motion of the spacecraft. The Sun and the Earth are selected as the two gravitational bodies for this investigation. The analysis of the relative motion between vehicles is expressed in an inertial coordinate frame. The reference trajectories employed in this investigation are first computed in a rotating frame relative to the primary bodies and then transposed in the inertial frame. A chief spacecraft is assumed to move along a given reference trajectory.

2.1. Relative motion described in the inertial frame

The equations of motion are described in an inertial coordinate frame where the spacecraft is located relative to the barycenter of the Sun and the Earth.Zhou et al. (2000) Let $\bar{X}$ define a general vector in the inertial frame describing the motion of the spacecraft, i.e.

$$\bar{X}(t) = [x \quad y \quad z \quad \dot{x} \quad \dot{y} \quad \dot{z}]^T \tag{1}$$

where superscript 'T' implies transpose. The dynamical system is defined as

$$\dot{\bar{X}}(t) = \bar{f}(\bar{X}, t) \tag{2}$$

The scalar nonlinear equations of motion in their non-dimensional forms expressed in the inertial frame are then written as

$$\ddot{x} = (1-\mu)(x_S - x)/r_{13}^3 + \mu(x_E - x)/r_{23}^3 \tag{3}$$

$$\ddot{y} = (1-\mu)(y_S - y)/r_{13}^3 + \mu(y_E - y)/r_{23}^3 \tag{4}$$

$$\ddot{z} = (1-\mu)(z_S - z)/r_{13}^3 + \mu(z_E - z)/r_{23}^3 \tag{5}$$

with

$$r_{13} = \sqrt{(x - x_S)^2 + (y - y_S)^2 + (z - z_S)^2} \tag{6}$$

$$r_{23} = \sqrt{(x - x_E)^2 + (y - y_E)^2 + (z - z_E)^2} \tag{7}$$

and where μ is the mass parameter associated with the Sun-Earth system. The positions of the Sun and the Earth are defined as (x_S, y_S, z_S) and (x_E, y_E, z_E), respectively. They are expressed as

$$x_S = -\mu\cos(t - t_0), \qquad x_E = (1-\mu)\cos(t - t_0) \tag{8}$$

$$y_S = -\mu\sin(t - t_0), \qquad y_E = (1-\mu)\sin(t - t_0) \tag{9}$$

$$z_S = 0, \qquad z_E = 0 \tag{10}$$

where the initial time is assumed to be zero, i.e., $t_0 = 0$. The right-hand side of Equation 3-5 can be expanded to first-order in μ as

$$\ddot{x} = -x/r^3 + \mu F(x, y, z, t, t_0) + O(\mu^2) \tag{11}$$

$$\ddot{y} = -y/r^3 + \mu G(x, y, z, t, t_0) + O(\mu^2) \tag{12}$$

$$\ddot{z} = -z/r^3 + \mu H(x, y, z, t, t_0) + O(\mu^2) \tag{13}$$

where $r = \sqrt{x^2 + y^2 + z^2}$, and

$$\begin{aligned} F(x, y, z, t, t_0) = & \frac{x - \cos(t - t_0)}{r^3} \\ & + \frac{3x(x\cos(t - t_0) + y\sin(t - t_0))}{r^5} \\ & + \frac{\cos(t - t_0) - x}{((x - \cos(t - t_0))^2 + (y - \sin(t - t_0))^2 + z^2)^{3/2}} \end{aligned} \tag{14}$$

$$\begin{aligned} G(x, y, z, t, t_0) = & \frac{y - \sin(t - t_0)}{r^3} \\ & + \frac{3y(x\cos(t - t_0) + y\sin(t - t_0))}{r^5} \\ & + \frac{\sin(t - t_0) - y}{((x - \cos(t - t_0))^2 + (y - \sin(t - t_0))^2 + z^2)^{3/2}} \end{aligned} \tag{15}$$

$$H(x,y,z,t,t_0) = \frac{z}{r^3} + \frac{-z}{((x-\cos(t-t_0))^2 + (y-\sin(t-t_0))^2 + z^2)^{3/2}} \quad (16)$$

The design process relies on variations relative to a reference trajectory. Given a solution to the nonlinear differential equations, linear variational equations of motion are derived from a first-order Taylor expansion defined as

$$\delta\dot{\bar{X}}(t) \approx \frac{\partial \bar{f}}{\partial \bar{X}}_{|\bar{X}-\bar{X}_{ref}} \delta\bar{X}(t) + \frac{\partial \bar{f}}{\partial t}_{|t-t_{ref}} \delta t + O(\delta\bar{X}^2, \delta t^2) \quad (17)$$

where $\delta\bar{X}(t) = \bar{X}(t) - \bar{X}_{ref}(t) = [\delta x \quad \delta y \quad \delta z \quad \delta\dot{x} \quad \delta\dot{y} \quad \delta\dot{z}]^T$ and $\delta t = t - t_{ref}$ represents variations about a reference trajectory. In this investigation, the variational equations are employed to describe the motion of a deputy vehicle relative to a chief spacecraft located on the reference path at the same time. Hence, the variation in time is assumed to be zero, i.e., $\delta t = 0$. The variational equations become

$$\delta\dot{\bar{X}}(t) \approx \frac{\partial \bar{f}}{\partial \bar{X}}_{|\bar{X}-\bar{X}_{ref}} \delta\bar{X}(t) = A(t)\delta\bar{X}(t) \quad (18)$$

where the $A(t)$ matrix is written in matrix form as

$$A(t) = \begin{bmatrix} 0_{3\times3} & I_{3\times3} \\ \tilde{U} & 0_{3\times3} \end{bmatrix} \quad (19)$$

2.2. Reference trajectories derived in the rotating frame

More generally, in the context of the CR3BP, the equations of motion are expressed in a rotating frame relative to the primary bodies. In the rotating frame, some structure can be identified such as equilibrium points, periodic and quasi-periodic orbits. One well-known type of periodic trajectory is the set of halo orbit families that are symmetric across the $(\hat{x}, \hat{z})$ rotating plane. These orbits are of particular interest and frequently serve as baseline trajectories for mission design. The northern halo orbit family near the L_2 Sun-Earth libration point appears in Figure 1. Two halo orbits with different amplitudes are selected in this family as reference trajectories for this investigation. The reference orbits appear in dark blue in Figure 1. They are denoted as either 'small' or 'large' reference orbits throughout this analysis

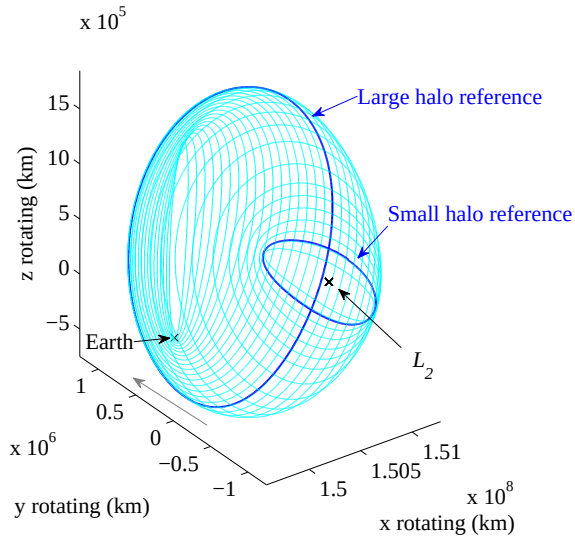

Figure 1: Northern halo family near the L_2 Sun-Earth libration point

Table 1: Amplitudes A_y and A_z of the two selected reference orbits

Reference orbits	Amplitude $A_y(km)$	Amplitude $A_z(km)$
Small halo reference	680,000	150,000
Large halo reference	1,000,000	2,000,000

to distinguish them. The approximative amplitudes A_y and A_z along the $\hat{y}$ and $\hat{z}$ axes, respectively, are listed in Table 1. These reference trajectories expressed in the rotating frame are transformed in the inertial frame via a rotation matrix, denoted T, that is defined as

$$\bar{X}_{rot}(t) = T^{-1}\bar{X}(t) \tag{20}$$

where

$$T = \begin{bmatrix} C & 0_{3\times 3} \\ \dot{C} & C \end{bmatrix} \tag{21}$$

with

$$C = \begin{bmatrix} \cos(t) & -\sin(t) & 0 \\ \sin(t) & \cos(t) & 0 \\ 0 & 0 & 1 \end{bmatrix} \tag{22}$$

$$\dot{C} = \begin{bmatrix} -\sin(t) & -\cos(t) & 0 \\ \cos(t) & -\sin(t) & 0 \\ 0 & 0 & 0 \end{bmatrix} \tag{23}$$

3. Natural regions suitable for small formations

The objective in this investigation is a better understanding of the dynamical environment at small distances from a specified reference path. A chief spacecraft evolves along a given reference trajectory represented in Figure 1. To describe the position of a deputy vehicle relative to the chief spacecraft, spheres of points at each time along the reference orbit are defined as illustrated in Figure 2. The spheres are enlarged in the figure for illustration, and their actual radius reflects a specified baseline distance that is assumed between the vehicles. At each time along the reference, the chief spacecraft is positioned at the center of a sphere. A deputy vehicle is then located somewhere on the surface of the sphere. A vector defined from the chief spacecraft to the deputy vehicle defines a direction or orientation for the formation. Every direction on the sphere is investigated at each time along the reference orbit and some specific directions on the spheres are derived that represent suitable locations to maintain small formations.

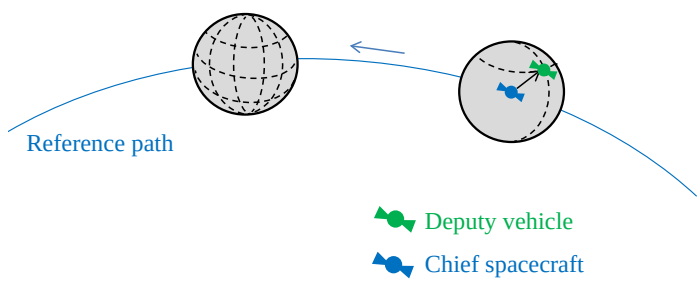

Figure 2: Spheres of test points relative to the chief spacecraft along the chief reference trajectory (enlarged size for illustration)

3.1. Low drift regions derived via variational equations

Natural regions close to the given chief reference path are derived to maintain small formations of spacecraft. Ideally, regions with zero relative velocity and zero relative acceleration maintain the mutual distance between

the spacecraft and the pointing direction orienting the formation.(Héritier & Howell, 2012) Assuming that the separation between the spacecraft is "small", no greater than a few kilometers at most, regions of low drift are derived via the first-order variational equations defined in Equation 18, with respect to the given reference orbit. These variational equations are rewritten in terms of three-dimensional relative position and relative velocity vectors as

$$\begin{bmatrix} \delta\dot{\bar{r}} \\ \delta\ddot{\bar{r}} \end{bmatrix} = \begin{bmatrix} 0_{3\times3} & I_{3\times3} \\ \tilde{U} & 0_{3\times3} \end{bmatrix} \begin{bmatrix} \delta\bar{r} \\ \delta\dot{\bar{r}} \end{bmatrix} \tag{24}$$

where $\delta\bar{r} = [\delta x \quad \delta y \quad \delta z]^T$ and $\delta\dot{\bar{r}} = [\delta\dot{x} \quad \delta\dot{y} \quad \delta\dot{z}]^T$. For the spacecraft placed at a small distance with respect to each other, the relative velocity in an ideal direction is assumed to be zero, i.e., $\delta\dot{\bar{r}} = \bar{0}$. Notice that this assumption is only valid for a small formation of spacecraft. At larger distances, the relative velocity may not be negligible. The goal in this investigation is the identification of some natural regions, on the sphere, that is, natural directions or orientations, that not only maintain the mutual distance between the spacecraft but also the orientation of the formation. Assuming no relative velocity between the spacecraft, regions that also possess zero relative acceleration would ideally maintain the formation. The norm of the relative acceleration is computed from the dot product of $\delta\ddot{\bar{r}}$ with $\delta\ddot{\bar{r}}$, i.e.,

$$\|\delta\ddot{\bar{r}}\|^2 = \delta\ddot{\bar{r}} \cdot \delta\ddot{\bar{r}} = \tilde{U}\delta\bar{r} \cdot \tilde{U}\delta\bar{r} \tag{25}$$

The locations such that the relative acceleration is equal to zero are then the set of points that satisfy the equation

$$\delta\bar{r}^T\tilde{U}^T\tilde{U}\delta\bar{r} = 0 \tag{26}$$

The analytical expression defined in Equation 26 represents regions with zero relative acceleration. Placing spacecraft in these low drift regions avoids large variations in their mutual distances while maintaining the orientation of the small formation. As the relative acceleration between the spacecraft never precisely reaches zero, a small positive coefficient, denoted ϵ, is introduced for the computation of the low drift regions. Equation (26) is then rewritten as

$$\delta\bar{r}^T\tilde{U}^T\tilde{U}\delta\bar{r} \leq \epsilon \tag{27}$$

The ϵ coefficient corresponds to the desired maximum value for the relative acceleration in the low drift region. Depending on the value for ϵ, the low

drift region can cover a smaller or larger portion of the sphere.

To numerically compute the low drift regions, a location along the reference trajectory is first selected that represents the state of the chief spacecraft. Relative to this location, a sphere of points that corresponds to a radius equal to 0.1 km is defined. Such a sphere of points is illustrated in Figure 3. The center of the sphere represents the selected location on the reference arc, i.e., the location of the chief spacecraft. The test points are parametrized by two angles, an in-plane angle θ measured from the $\hat{x}$-axis in the inertial frame and an out-of-plane angle β defined relative to the ($\hat{x}$, $\hat{y}$)-plane. The velocity of all the points on the sphere is assumed to be equal

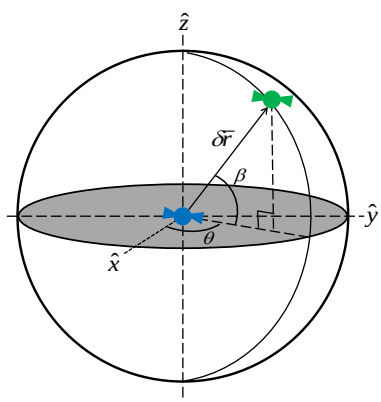

Figure 3: Sphere of test points described by in-plane angle θ and out-of-plane angle β

to the velocity of the selected location on the reference trajectory in this linear analysis since $\delta\dot{\bar{r}}$ is assumed as zero. The relative acceleration that corresponds to each of the states on the sphere is evaluated using the right side of Equation (25), and the states on the sphere that possess the smallest values for the relative acceleration represent the low drift regions.

To illustrate how the relative acceleration varies with respect to the relative directions on the sphere, the relative acceleration between the spacecraft is investigated at one location along the reference trajectory. One specific location along the large halo reference orbit, identified as time $t = 109$ days along the reference path, is selected and represents the state for the chief spacecraft. A set of test points on a sphere of radius 0.1 km is defined around this location, and the norm square of the relative acceleration for each of these points is evaluated using the right side of Equation (25). The norm square of the relative acceleration is then plotted as a function of the

two angles θ and β defined previously in Figure 3. The surface of relative acceleration at time $t = 109$ days along the large halo reference orbit is represented in Figure 4. This surface possesses two minima located at (β = -24 deg, $\theta = 77$ deg) and ($\beta = 27$ deg, $\theta = 260$ deg), respectively. These minima represented in pink correspond to the low drift region. The corresponding sphere of points at time $t = 109$ days along the reference orbit is illustrated in Figure 5. The colors on the sphere reflect the value of the relative acceleration at the specific locations on the sphere. The locations colored in pink on the sphere correspond to the low drift region, that is where the relative acceleration has the smallest values.

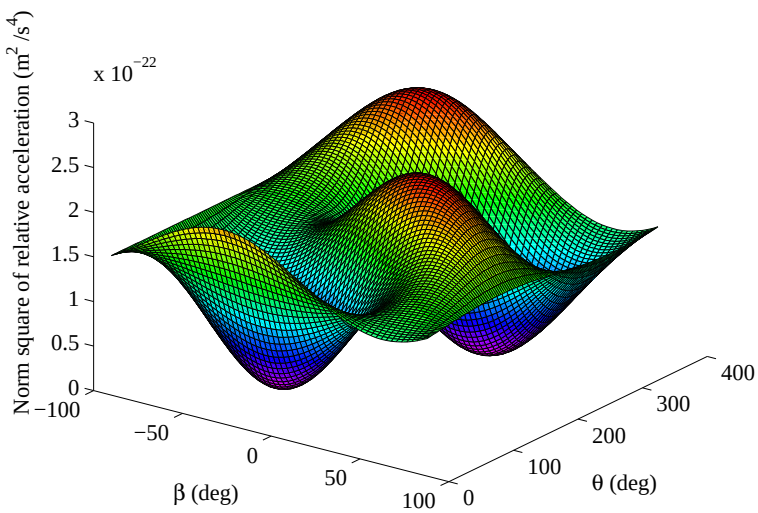

Figure 4: Surface of the norm square of the relative acceleration at the location that is identified as $t = 109$ days from the initial location along the large reference orbit

3.2. Dynamic behavior within the low drift regions

Directions for the formation that correspond to the low drift regions are compared with the other directions on a given sphere. Placing a deputy vehicle on the sphere surface in the low drift zone avoids large variations in the mutual distance between the spacecraft while maintaining the orientation of the formation. First, a state at time $t = 109$ days along the large reference trajectory is selected. This state represents the initial location of the chief spacecraft. Then, a set of test points on a sphere of radius 0.1 km around this location is generated. These test points correspond to the initial locations

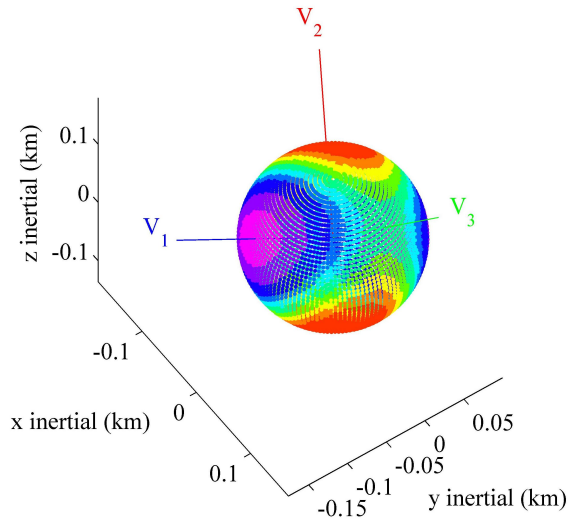

Figure 5: Sphere of test points colored by relative acceleration at the chief location that is identified as $t = 109$ days from the initial location along the large reference orbit

for the deputy vehicle. Initially, the deputy vehicle is placed either in the orientation of the low drift region or in the other directions on the sphere, at a distance of 0.1 km from its chief spacecraft. Then, the paths of both spacecraft are integrated for an interval of time of 10 days as an illustration. The natural drift is then calculated by considering the variation of the formation, both in magnitude and orientation after the 10 days. The schematic in Figure 6 represents the natural drift for the formation over the time interval $[t_0 \quad t_f]$. The deputy vehicle is assumed to possess the same velocity

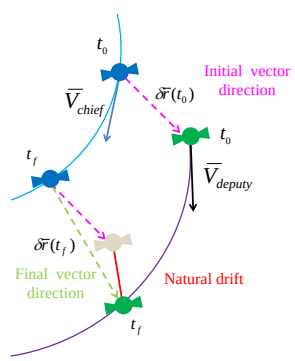

Figure 6: Schematic of the natural drift

vector as the chief spacecraft initially, i.e, $\bar{V}_{deputy} = \bar{V}_{chief}$. At each initial location for the deputy vehicle, either on the directions of low drift or on the other directions, the natural drift after 10 days is calculated and the results appear in Figure 7. The natural drift possess two minima that correspond to the same locations as the minima for the relative acceleration illustrated in Figure 4, that is the low drift region. For this particular simulation, as-

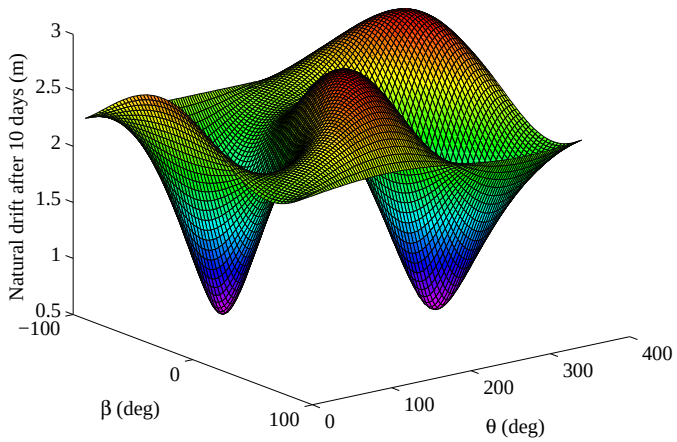

Figure 7: Natural drift after 10 days for a 1-km formation placed either along the unstable/stable directions or on the low drift region

suming an initial distance between the two vehicles of 0.1 km, the natural drift is determined to be less than 0.6 km if the deputy vehicle is initially located in the low drift zone represented in pink in Figure 7. The natural drift can reach about 3 km if the deputy is located in the red region, that is the region that possesses the highest relative natural drift. If the mutual distance between the spacecraft gets larger or if the time of integration for this simulation increases, the natural drift increases and the formation can experience larger deviations.

4. Low drift regions as quadric surfaces

By considering the analytical expression for the low drift zones derived in Equation 27, it is apparent that these low drift regions are represented as quadric surfaces. Using a change in coordinate, Equation 27 is transformed into its canonical form. The singular value decomposition of $\tilde{U}$ then takes

the form

$$\tilde{U} = P\Delta P^T = \begin{bmatrix} \bar{V}_1 & \bar{V}_2 & \bar{V}_3 \end{bmatrix} \begin{bmatrix} \lambda_1 & 0 & 0 \\ 0 & \lambda_2 & 0 \\ 0 & 0 & \lambda_3 \end{bmatrix} \begin{bmatrix} \bar{V}_1 & \bar{V}_2 & \bar{V}_3 \end{bmatrix}^T \tag{28}$$

where Δ is a real diagonal matrix with λ_1, λ_2 and λ_3, the eigenvalues of $\tilde{U}$, on its diagonal. Then, P is an orthogonal matrix with columns $\bar{V}_1, \bar{V}_2$ and $\bar{V}_3$ that represent the eigenvectors of $\tilde{U}$. These eigenvectors form an orthogonal basis and identify the principal directions of the quadric surface. Define a new vector $\bar{y} = [y_1 \quad y_2 \quad y_3]^T$ such that $\bar{y} = P^T\delta\bar{r}$. Equation 27 is then rewritten in the following canonical form

$$\bar{y}^T P^T \tilde{U}^T \tilde{U} P \bar{y} = \bar{y}^T \Delta^2 \bar{y} = \lambda_1^2 y_1^2 + \lambda_2^2 y_2^2 + \lambda_3^2 y_3^2 \leq \epsilon \tag{29}$$

Equation 29 represents an algebraic equation of degree two. In general, an equation of the second degree represents one of 17 different canonical forms that correspond to 17 canonical surfaces.(Hilbert & Cohn-Vossen, 1999) The specific type of quadric surfaces then depends on the given reference orbit and its corresponding eigenstructure. The quadric surfaces derived along the reference paths in this investigation are ellipsoids.

To derive these ellipsoids, various distances between the chief spacecraft and the deputy vehicle are examined, from 0.05 km to 2 km, while maintaining a constant value for the ϵ coefficient. Ellipsoids along the small reference trajectory are illustrated in Figure 8. One ellipsoid at time $t = 20$ days along the reference path appears in Figure 9. The size of the ellipsoids is enlarged for illustration in the figure. The eigenvectors of the $\tilde{U}$ matrix, that is, $\bar{V}_1, \bar{V}_2$ and $\bar{V}_3$, corresponding to the respective eigenvalues are also plotted in Figures 8 and 9. They represent the three principal directions corresponding to the ellipsoids. These ellipsoids represent regions of minimum relative acceleration, that are regions with low natural drift. Placing a formation of spacecraft on these ellipsoids maintain relatively well the distance between the spacecraft and the orientation of the formation. To investigate the effect of the reference path on the ellipsoids, the ellipsoids are also determined along the large reference halo orbit and they appear in Figures 10 and 11. These ellipsoids possess the same maximum relative acceleration, i.e., the same ϵ coefficient as the ones along the small reference path illustrated in Figures 8. Notice that, given the same value of the ϵ coefficient, the ellipsoids derived along the two reference trajectories have a significant different

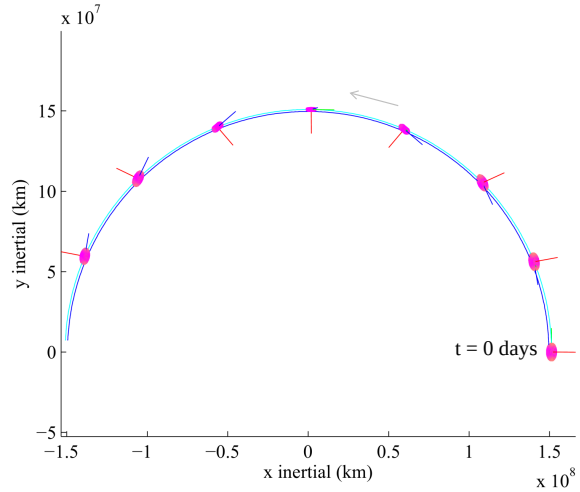

Figure 8: Quadric surfaces along the small reference halo orbit in the inertial frame (enlarged size for illustration)

size, shape and orientation and, therefore, depend highly on the reference trajectory selected.

5. Transient behavior along the reference paths

The dynamical evolution of the quadric surfaces and the eigenstructure of the reference trajectories are examined in details. To aid in the interpretation of the orientation and shape of the quadric surfaces, it is convenient to represent the ellipsoids in the rotating frame of the primaries. The ellipsoids along the two reference halo orbits are transposed in the rotating frame and appear in Figures 12 and 13. In these figures, the close proximity of the Earth leads to a higher level of sensitivity and, therefore, to a smaller size of the low natural drift regions. In particular, the bottom side of the large reference halo orbit represented in Figure 13 is in closest proximity with the Earth. As a consequence, no regions of low drift are analytically indicated in the vicinity of this portion of the orbit.

The evolution of the eigenvalues of the $\tilde{U}^T\tilde{U}$ matrix over one period of the two reference paths appears in Figure 14(a) and Figure 14(b), respectively. Along the small reference trajectory, the magnitudes of the eigenvalues remain relatively constant over time. As the reference orbit gets larger and closer to the Earth, the region in its vicinity becomes more sensitive and

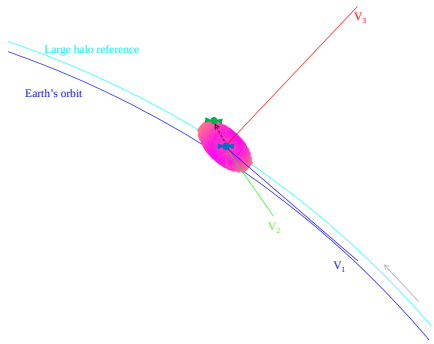

Figure 9: One quadric surface at time $t = 20$ days along the small reference halo orbit in the inertial frame

more variations in the eigenvalues is noticeable. Over the time interval that surrounds time $t = 90$ days in Figure 14(b), the magnitude of the three eigenvalues gets noticeably larger. This peek in magnitude is due to the proximity of the Earth. At this location, the relative velocity and relative acceleration between the spacecraft are higher and, therefore, no low drift regions are expected near this location since the chief is passing too close to the Earth.

6. Summary and concluding remarks

In this present investigation, the natural dynamics in the L_2 Sun-Earth libration point region are exploited to aid in the control of a formation of spacecraft. Natural zones that exhibit low relative drift are derived such that large variations in the mutual distances between the spacecraft are prevented while maintaining the orientation of the formation. For small formations, these low drift regions represent quadric surfaces and they are derived analytically using variational equations with respect to the reference trajectory. These regions of low drift depend highly on the reference trajectory. In particular, the type of quadric surfaces and their orientation is determined by the eigenstructure along the reference path. Moreover, if the reference trajectory is located in a sensitive region, for example a region such that the chief spacecraft passes close to either primary, the eigenvalues along the reference path tend to increase significantly in magnitude and no zones with zero relative velocity exist via linear analysis.

Further exploration of the natural dynamics in the Sun-Earth system or other systems may be examined for the placement of a formation of space-

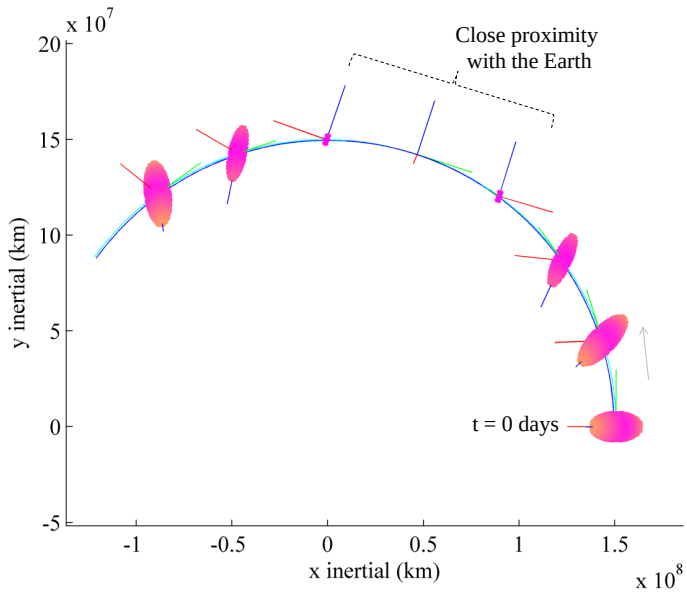

Figure 10: Quadric surfaces along the large reference halo orbit in the inertial frame (enlarged size for illustration)

craft. This current analysis focuses essentially on the L_2 Sun-Earth halo orbits for reference trajectories but other reference orbits may be exploited for formation flying such as vertical, axial or resonant orbits, as well as unstable and stable manifold arcs for transfer trajectories of multiple spacecraft. By investigating different environments or various reference trajectories, some potential new characteristics for the low drift regions may be determined.

References

Zhou, J.L., Sun, Y.S., Zheng, J.Q., Valtonen, M.J., The transfer of comets from near-parabolic to short-period orbits: map approach, Journal of Astronomy and Astrophysics, 364, 887-893, 2000.

Barten, B.T., Howell, K.C., Fundamental motions near collinear libration points and their transitions, Journal of the Astronautical Sciences, 46(4), 361-378, 1998.

Cash, W., the New Worlds Team, The New Worlds Observer: the astrophysics strategic mission concept study, EPJ Web of Conferences, 16(07004), doi:10.1051/epjconf/20111607004, 2011.

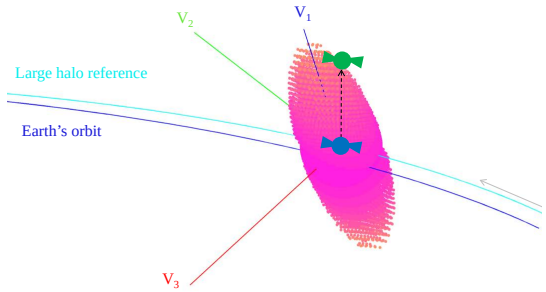

Figure 11: One quadric surface at time $t = 20$ days along the large reference halo orbit in the inertial frame

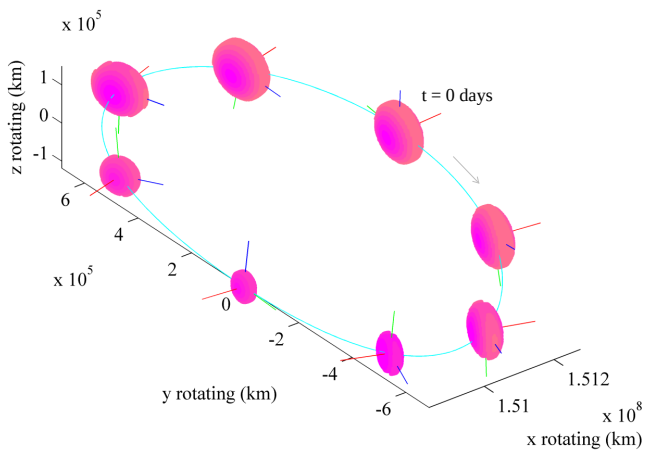

Figure 12: Ellipsoids along the small reference halo orbit in the rotating frame (enlarged for illustration)

Gómez, G., Lo, M., Masdemont, J., Museth, K., Simulation of formation flight near L2 for the TPF mission, AAS Astrodynamics Specialist Conference, Quebec City, Canada, paper no. AAS 01-305, 2001.

Gómez, G., Marcote, M., Masdemont, J., Mondelo, J., Zero relative radial acceleration cones and controlled motions suitable for formation flying, Journal of the Astronautical Sciences, 53(4), 413-431, 2005.

F.Y. Hsiao, F.Y., Scheeres, D.J., Bifurcations and Dynamical Evolution of Eigenvalues of Hamiltonian Systems, Physica D, 213, 66-75, 2006.

Héritier, A., Howell, K.C., Natural regions near the Sun-Earth libration

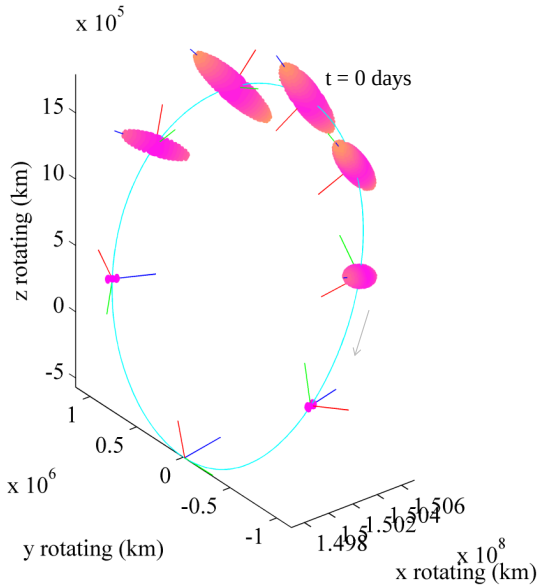

Figure 13: Ellipsoids along the large reference halo orbit in the rotating frame (enlarged for illustration)

points suitable for space observations with large formations, AAS/AIAA Astrodynamics Specialist Conference, Girwood, Alaska, paper no. AAS 11-493, 2011.

Héritier, A., Exploration of the region near the Sun-Earth collinear libration points for the control of large formations, Ph.D. Thesis, Purdue University, West Lafayette, Indiana, 2012.

Héritier, A., Howell, K.C., Regions Near the Libration Points Suitable to Maintain Multiple Spacecraft, AAS/AIAA Astrodynamics Specialist Conference, Minneapolis, Minnesota, paper no. AAS 12-4666, 2012.

Hilbert, D., Cohn-Vossen, S., The second-order surfaces, Geometry and Imagination, 3, 12-19, 1999.

Hsiao, F.Y., Scheeres, D.J., Stabilizing motion relative to an unstable orbit: applications to spacecraft formation flight, Journal of Guidance, Control, and Dynamics, 26(1), 2003.

Hsiao, F.Y., Scheeres, D.J., Design of spacecraft formation orbits relative

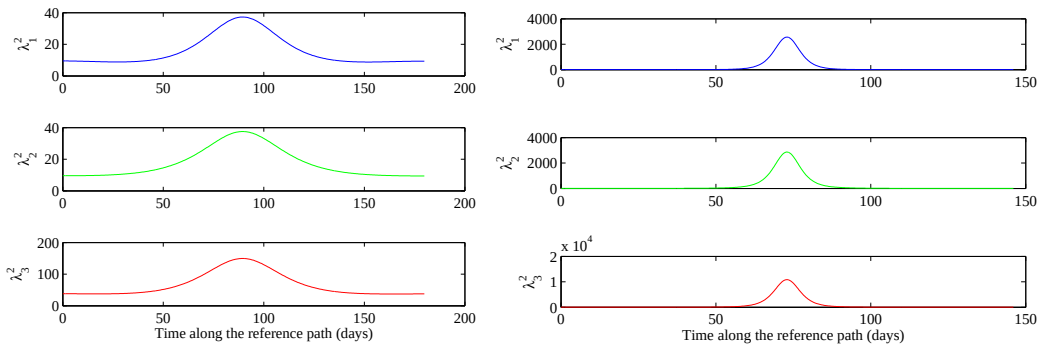

(a) (b)

Figure 14: Dynamical evolution of the eigenvalues of $\tilde{U}^T\tilde{U}$; (a) along the small reference halo orbit; (b) along the large reference halo orbit

to a stabilized trajectory, Journal of Guidance, Control, and Dynamics, 28(4), 2005.

Kolemen, E., Kasdin, J., Optimal trajectory control of an occulter-based planet-finding telescope, Advanced in Astronautical Science, 128, 215-233, paper no. AAS 07-037, 2007.

Lo, M., External occulter trajectory study, NASA JPL, September, 2006.

Luquette, R., Sanner, R., Spacecraft formation control: managing line-of-sight drift based on the dynamics of relative motion, 3rd Int. Symp. Formation Flying, Missions, and Technologies, Noordwijk, The Netherlands, 2008.

Marchand, B.G., Howell, K.C., Natural and non-natural spacecraft formations near the L1 and L2 libration points in the Sun-Earth/Moon ephemeris system, Dynamical Systems: an International Journal, Special Issue: Dynamical Systems in Dynamical Astronomy and Space Mission Design, 20(1), 149-173, 2005.

Marchand, B.G., Howell, K.C., Control strategies for formation flight in the vicinity of the libration points, Journal of Guidance, Control, and Dynamics, 28(6), 1210-1219, 2005.

Millard, L., Howell, K.C., Optimal reconfiguration maneuvers for spacecraft imaging arrays in multi-body regimes, Acta Astronautica, 63(11-12), 1283-1298, doi: 10.1016/j.actaastro.2008.05, 2008.

Millard, L., Howell, K.C., Control of spacecraft occulter arrays in multi-body regimes, AAS/AIAA Astrodynamics Specialists Conference, Honolulu, Hawaii, 2008.

Virgili, L.P., Design and evaluation of navigation and control algorithms for spacecraft formation flying missions, Ph.D. Thesis, Universitat de Barcelona, Barcelona, Spain, 2006.